GEOPHYSICS, VOL. 78, NO. 2 (MARCH-APRIL 2013); P. WA3–WA14, 22 FIGS.
10.1190/GEO2012-0294.1

Downloaded 09/15/21 to 69.181.137.94. Redistribution subject to SEG license or copyright; see Terms of Use at http://library.seg.org/page/policies/terms
DOI:10.1190/geo2012-0294.1

Broadband seismic data — The importance of low frequencies

Fons ten Kroode[1], Steffen Bergler[2], Cees Corsten[3], Jan Willem de Maag[1], Floris Strijbos[1], and Henk Tijhof[1]

ABSTRACT

We considered the importance of low frequencies in seismic reflection data for enhanced resolution, better penetration, and waveform and impedance inversion. We reviewed various theoretical arguments underlining why adding low frequencies may be beneficial and provided experimental evidence for the improvements by several case studies with recently acquired broadband data. We discussed where research and development efforts in the industry with respect to low frequencies should be focusing.

INTRODUCTION

Recent industry developments in seismic acquisition technology (Hill et al., 2006; Moldoveanu et al., 2006; Carlson et al., 2007a, 2007b; Tenghamn et al., 2007; Baigani, 2008; Baeten et al., 2010, Soubaras, 2010; Soubaras and Dowle, 2010; Parkes and Hegna, 2011; Caprioli et al., 2012; Wei et al., 2012) have enabled the acquisition of broader bandwidth seismic data. Higher frequencies provide a sharper wavelet, whereas the extension to lower frequencies reduces the side lobes of the wavelet. Lower frequencies also suffer less from scattering and attenuation in the earth and can therefore penetrate deeper. Moreover, they play an important role in seismic inversion for velocity and impedance models. The potential advantages of broader bandwidth seismic acquisition can therefore be largely grouped into three categories: (1) higher-resolution seismic images, (2) better signal penetration, and (3) better suitability for seismic inversion.

The methodologies to acquire broader bandwidth data vary. In marine seismic acquisition, the free surface reflection or "ghost" limits the effective bandwidth through destructive interference with the direct arrival. The frequencies at which this occurs depend on streamer depth, the direction of wave propagation, and the water velocity. All acquisition and processing methods to date attempt to remove this destructive interference on the receiver side, leading, in combination with the use of high-fidelity streamers, to so-called broadband data. More recently, we have also seen methods to address the ghost reflection on the marine source side using different approaches. On land, new vibrator technology has extended the bandwidth in particular to the lower frequencies.

In this paper, we are not comparing the advantages of different acquisition and processing approaches, but we are reviewing the relevance of broader bandwidth seismic data for our business. From experiments with onshore and offshore data, we see the largest impact through the addition of lower frequency energy, and in this paper we explore reasons for this. First, we investigate the importance of the low frequencies to improve resolution. Second, we analyze the effect of the low frequencies on wavefield scattering and penetration. Third, we look at inversion techniques — full waveform inversion and impedance inversion — using the low frequencies. We conclude with a discussion on the further implications of these observations, including the direction for further developments.

RESOLUTION

The importance of broadband data acquisition and processing needs to be justified by the usability of low and high frequencies in the final seismic interpretation product. Improving the resolution of the wavelet, i.e., separation between two seismic events by reducing the width of the main lobe of the wavelet, can be achieved by increasing the bandwidth at the high-frequency end. Adding bandwidth at the low-frequency end reduces the wavelet sidelobe amplitude (see, e.g., Kallweitt, 1982) and reduces potential interference with neighboring events. Figure 1 compares four Butterworth band-pass filter impulse responses with different low-cut frequency (2, 4, 8, and 16 Hz). The increasing low-cut frequency results in

Manuscript received by the Editor 27 July 2012; published online 20 March 2013.
[1]Shell Global Solutions International, Rijswijk, The Netherlands. E-mail: a.tenkroode@shell.com; jw.demaag@shell.com; floris.strijbos@shell.com; henk.tijhof@shell.com.
[2]Brunei Shell Petroleum Company Sdn. Bhd, Seria, Brunei Darussalam. E-mail: steffen.bergler@shell.com.
[3]A/S Norske Shell, Tananger, Norway. E-mail: c.corsten@shell.com.
© 2013 Society of Exploration Geophysicists. All rights reserved.

Downloaded 09/15/21 to 69.181.137.94. Redistribution subject to SEG license or copyright; see Terms of Use at http://library.seg.org/page/policies/terms
DOI:10.1190/geo2012-0294.1

increasing sidelobe amplitudes. A similar reduction in sidelobe strength can be achieved by changing the slope of the passband. Figure 2 shows that the 5–45-Hz impulse response of the Butterworth filters with a −3 dB/octave and a 0 dB/octave slope on the passband have quite different sidelobe amplitudes. The peak-to-sidelobe ratio improves from 3.5 for the 0 dB/octave wavelet to 10.0 for the −3 dB/octave wavelet. Notice that emphasizing the low frequencies in this manner is only possible if the signal-to-noise ratio (S/N) at the low end of the spectrum is good enough.

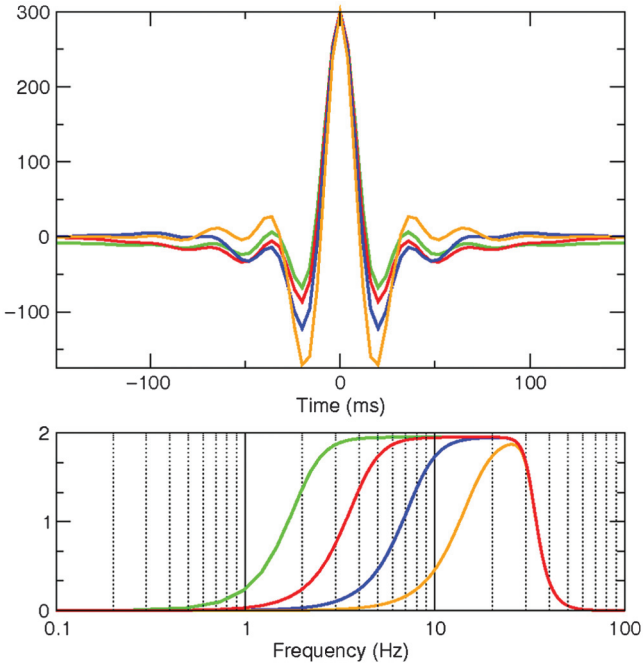


Figure 1. Butterworth filter high cut 32 Hz and 12 dB/octave low cut at 2 (green), 4 (red), 8 (blue), and 16 Hz (yellow).

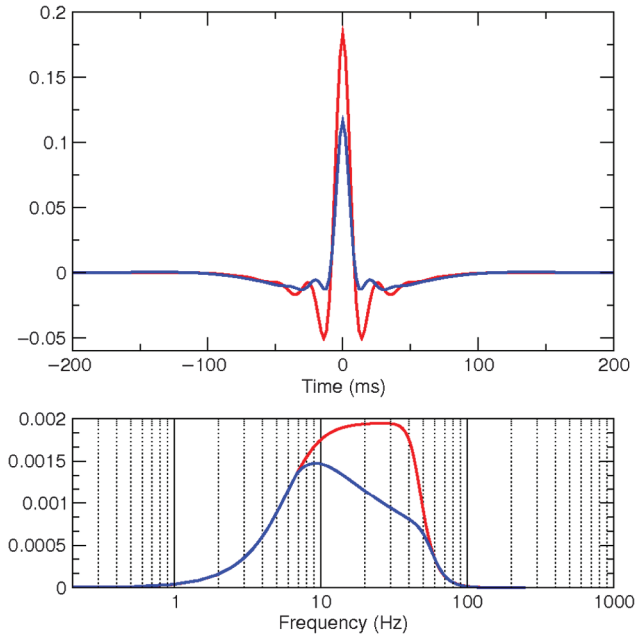


Figure 2. A 5–45-Hz Butterworth filter with changing slopes of passband (−3 dB/octave [blue] and 0 dB/octave [red]). Time-domain signature (top) and spectrum (linear amplitude versus logarithmic frequency). The peak-to-sidelobe ratio improves from 3.5 for the red wavelet to 10.0 for the blue wavelet.

To further investigate the importance of low-frequency data, we will use the Butterworth wavelet with a slope of −3 dB/octave (blue curve in Figure 2). This input wavelet is shown as the first trace in Figure 3a. The other traces show a *wedge model*, i.e., the interference of the input wavelet convolved with a positive spike followed by a negative spike of equal strength while changing the time delay between the two reflections from 51 to 6 ms. We see that the resulting waveform shows two distinct reflections without strong sidelobes. However, if we apply a 90° phase rotation to construct a band-limited impedance wavelet (Figure 3b) we see strong sidelobe amplitudes on the resulting waveform: the interference of two closely spaced events with opposite phase approximates a differentiator and low frequencies are reduced by 6 dB/octave (Widess, 1973). To compensate for the loss in low frequencies, we boost the low frequencies by 6 dB/octave, and we see in Figure 3c that for the closely spaced events, the sidelobe amplitude is strongly reduced without any noticeable effect on the width of the central lobe.

It should be noted that this result is only achieved if the reflectivity wavelet has a −3 dB/octave emphasis, an additional −6 dB/octave boost is applied to the data, and the earth spectrum is white. Various authors have measured a −3 dB/octave emphasis on the spectrum of impedance logs and shaping an impedance trace to this trend may thus not result in the optimal wavelet.

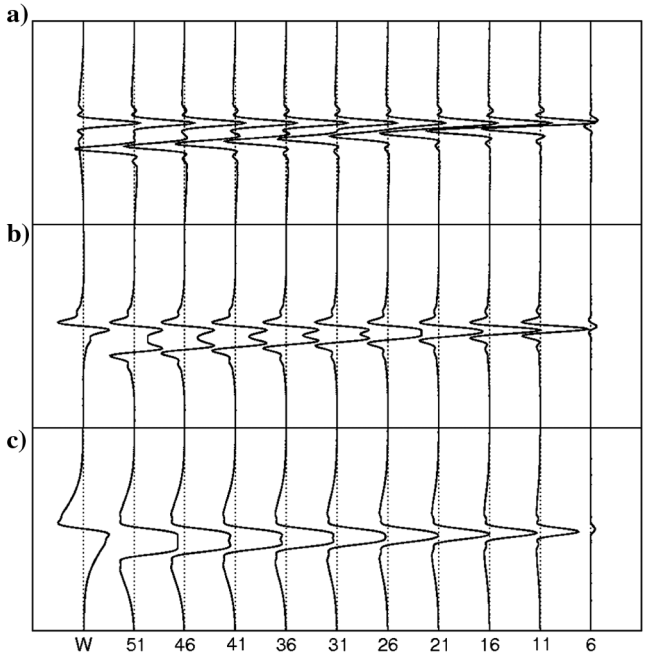


Figure 3. (a) Wedge model showing the interference of a positive and equal strength negative reflection at various time intervals. The time interval in milliseconds is indicated by the label. The first curve (indicated by "W") is the wavelet of a single reflection. (b) Same as (a), but with added 90° phase rotation (c) Same as (b), but with an additional 6 dB/octave boost of low frequencies.

Downloaded 09/15/21 to 69.181.137.94. Redistribution subject to SEG license or copyright; see Terms of Use at http://library.seg.org/page/policies/terms
DOI:10.1190/geo2012-0294.1

Figure 4a shows the potential improvement if we were able to reduce the lowest frequency from the typical 7 Hz for an airgun source (see Hegna et al., 2011) to 1 Hz. Figure 4b shows the optimized 7-Hz low-cut wavelet that has the sidelobes for the thinner part of the wedge reduced, but the thicker part still has a significant sidelobe. If we are able to reduce the lowest frequency to 1 Hz (Figure 4c), then the sidelobe for the thicker part of the wedge is also smaller.

These examples illustrate the effect on a reflection followed by a reflection of opposite sign. Similar improvements are achieved for more complicated waveforms. Figure 5 shows a waveform created out of several negative and positive amplitude events at 50-ms spacing. The amplitude spectrum (green curve) depicted in this plot shows a −6 dB/octave amplitude decay consistent with a white reflectivity spectrum. No sidelobes are present in the time series. If we match this spectrum over the passband of the band-limited data set (blue curve), we see that we still have significant sidelobes. The spectrum of the reflection response of recorded data has been observed to approximate +3 dB/octave and −3 dB/octave decay for the impedance response (Velzeboer, 1981). Shaping the spectrum to −3 dB/octave (black curve) to mimic this observed impedance spectrum results in severe sidelobes. Applying a −9 dB/octave slope to the wavelet (red curve) results in strongly reduced sidelobes.

Figures 6 and 7 show the same waveform at 25- and 10-ms event spacing, respectively. Although the envelope of the broadband spectrum shown in Figure 7 has a −6 dB/octave decay, the emphasis on the passband is clearly on the high frequencies and would explain why a seismic trace with a good distribution of the interval times can result in a nonwhite reflectivity spectrum. So if the spectrum of the reflectivity trace suggests a +3 dB/octave emphasis, the effective data wavelet may have a much stronger emphasis on the low frequencies and could benefit from further low-frequency

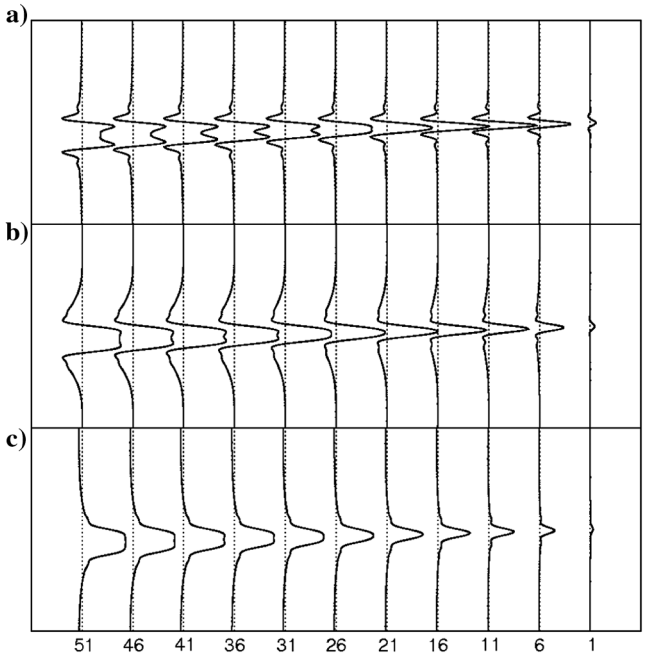


Figure 4. Wedge model showing the interference of a positive and equal strength negative reflection at various time intervals. (a) A 1–45-Hz Butterworth filter with a −2.5 dB/octave emphasis on the low frequencies is used as wavelet. The time interval in milliseconds is indicated by the label. (b) Same as (a), but with a 7-Hz low cut and an additional −6 dB/octave emphasis of the low frequencies (c) Same as (b), but with a 1-Hz low cut on the Butterworth filter.

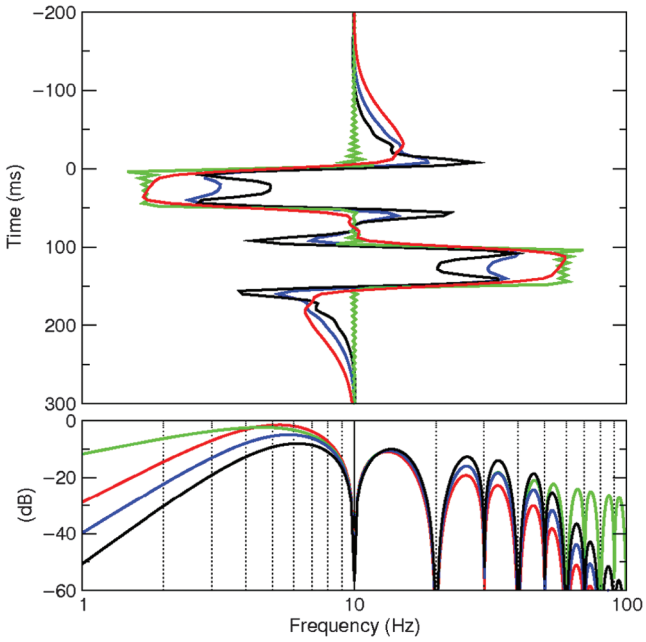


Figure 5. Waveform of a more complicated reflection with 50 ms between events: −3 dB/octave (black), −6 dB/octave (narrowband: blue), −6 dB/octave (broadband: green), and −9 dB/octave (red).

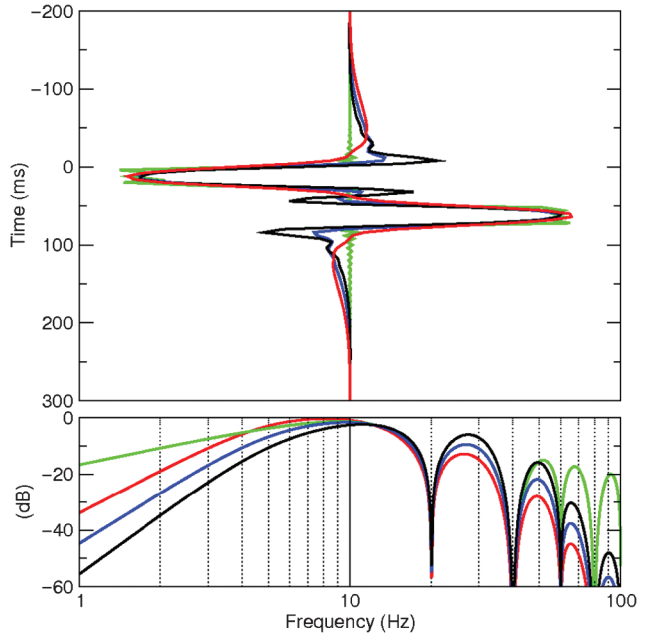


Figure 6. Same as Figure 5, but with 25 ms between events.

Downloaded 09/15/21 to 69.181.137.94. Redistribution subject to SEG license or copyright; see Terms of Use at http://library.seg.org/page/policies/terms
DOI:10.1190/geo2012-0294.1

enhancement to reduce sidelobe strength. As a consequence, amplitude and phase fidelity at the low frequencies are important to achieve an accurate interpretation. In our experience, phase fidelity of the low frequencies is generally poor in real data and needs further improvement.

With a 2D test line over a producing field, we will show the impact of low frequencies on the seismic interpretation. Figure 8 shows a comparison of 2D impedance data with 2D broadband data. The top reservoir reflector in this field is impacted by a high-impedance layer embedded in a low impedance formation such that

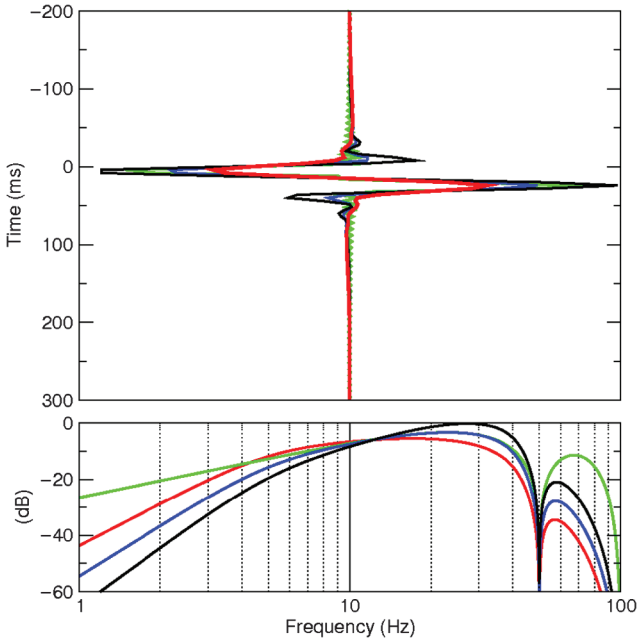


Figure 7. Same as Figure 5, but with 10 ms between events.

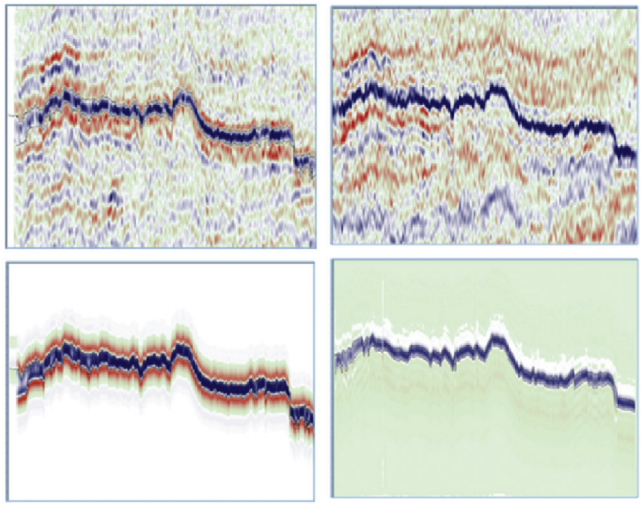


Figure 8. The 2D regular seismic data (top left), 2D broadband data (top right), synthetic from regular seismic wavelet (bottom left), and synthetic from wavelet derived from 2D broadband data (bottom right).

the sidelobe of this high-impedance contrast coincides with the top reservoir reflector. As can be seen in Figure 8 (top left), this results in a low-frequency shadow around the high-impedance layer (blue = high impedance, red = low impedance). A synthetic containing only the hard layer and generated with a wavelet derived from the inverted 2D data confirms this strong energy to be due to the high-impedance layer. On the right of Figure 8, we see the corresponding 2D broadband data and the synthetic data with the broadband derived wavelet. It is clear that the broadband 2D data contain sufficient low-frequency energy to avoid strong sidelobe energy.

The various synthetic data examples illustrate that additional low frequencies and the shape of the passband improve seismic resolution in terms of peak-to-sidelobe ratio. The loss of low frequencies when two reflectors of opposite sign interfere can be compensated by applying an additional 6 dB/octave emphasis on the low frequencies without significant loss in resolution for a more complicated series of reflections. With a real data example, we showed that the effect of the sidelobe of a strong reflector masking adjacent reflectors can be compensated for by emphasizing the low-frequency data. The optimized wavelet thus improves interpretation of seismic data for reflection and band-limited impedance data created by filtering of the reflectivity trace. We stress that emphasizing the low frequencies present in a data set can only be done if the S/N is good enough at the low end.

PENETRATION — SCATTERING AND ABSORPTION

Seismic waves can behave quite differently at low frequencies than at high frequencies. A scattering inhomogeneity in a background medium creates a scattered wavefield that is proportional to the product of the contrast and frequency squared:

$$P_{\text{scattered}} \sim (\text{frequency squared}) \times (\text{contrast}) \times (\text{total wavefield}). \quad (1)$$

The general Lippmann-Schwinger form of this formula (Lippmann and Schwinger, 1950) constitutes the basis of many approximations, such as the Born, Bremmer, Rytov, de Wolf, etc.; see, e.g., Bremmer (1951), Morse and Feshbach (1953), Aki and Richards (1980), and Wu (2003) for a historical review. In the case of weak scatterers, we replace the total wavefield by the incident wavefield and the relation above becomes

$$P_{\text{scattered}} \sim (\text{frequency squared}) \times (\text{contrast}) \times (\text{incident wavefield}). \quad (2)$$

This relation shows that the scattered wavefield is proportional to the ratio of the volume of the scatterer and the square of the wavelength of the incident wavefield, and when this ratio is small (i.e., for low frequencies or equivalently long wavelengths), the scattered wave is negligible to the incident wavefield. As a consequence, the low-frequency part of the wavefield is influenced very little by small scale inhomogeneities and propagates as if they were not present. This difference between wave propagation at low and at high frequencies can be strikingly illustrated by inserting a rugose 1700 m/s layer (the inhomogeneity) between two layers of 750 and 3000 m/s as in Figure 9 and inspecting the reflected wavefronts, as modeled by a finite-difference simulation of wave

Downloaded 09/15/21 to 69.181.137.94. Redistribution subject to SEG license or copyright; see Terms of Use at http://library.seg.org/page/policies/terms
DOI:10.1190/geo2012-0294.1

propagation from a source in the upper layer at low frequencies (10–15 Hz) and high frequencies (50–80 Hz) in Figure 10. The "rugosity" consists of a simple sinusoidal interface with wavelength 15 m and amplitude 7.5 m. Note that, for an incident wavefield velocity of 750 m/s, the low frequencies modeled correspond to wavelengths in the order of 50–75 m, whereas the high frequencies modeled correspond to wavelengths in the order of 10–15 m. The reflection data and the corresponding spectra indicate that the low-frequency wavelet reflection data from the 1750- to 3000-m/s interface are reflected and recorded virtually undisturbed by the rugose interface, as if it was not present, whereas the high-frequency wavelet reflection data and spectrum are heavily affected by it.

This effect also occurs in practice. In Figure 11, a thin, but rugose, high-velocity salt layer (in the very top of the section) affects the development of a coherent reflected wavefront from deeper sedimentary boundaries for high frequencies for conventional acquisition (top), but low frequencies of source-and-receiver broadband acquisition (bottom) penetrate through that layer as a coherent wavefront, almost as if it was not present.

Besides under rugose salt, this effect can also be observed below rugose basalt. In Figure 12, a thickening basalt layer seems to affect the deep reflector almost abruptly below the pinch-out of the basalt for conventional acquisition. For broadband acquisition, the event shows an improved bandwidth and shows more continuity below the pinch-out of the basalt, but is eventually breaking up when the basalt is thickening. Besides this, other events become visible below the basalt on the broadband section, in particular, base basalt (indicated by arrows in Figure 12) is a clearly interpretable event, which can only be inferred on the conventional data.

The generally accepted formula for absorption of acoustic waves indicates that the effect of absorption is less for the lower frequencies than for the higher frequencies, and therefore, it is generally assumed that penetration to deeper layers is better for

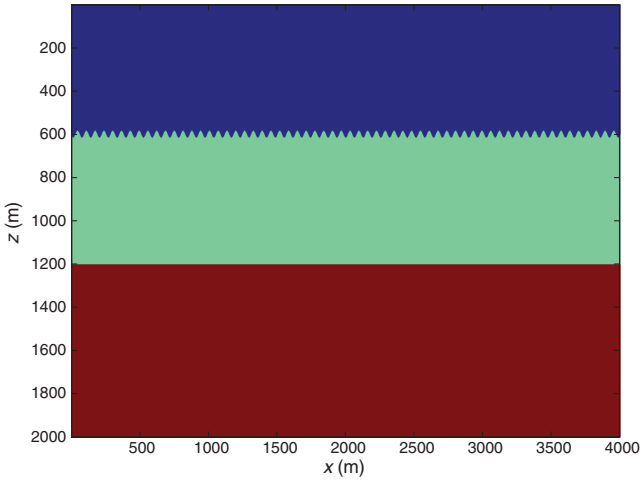


Figure 9. Velocity model with a rugose 1700 m/s layer, in between a 750 m/s layer and a 3000 m/s layer.

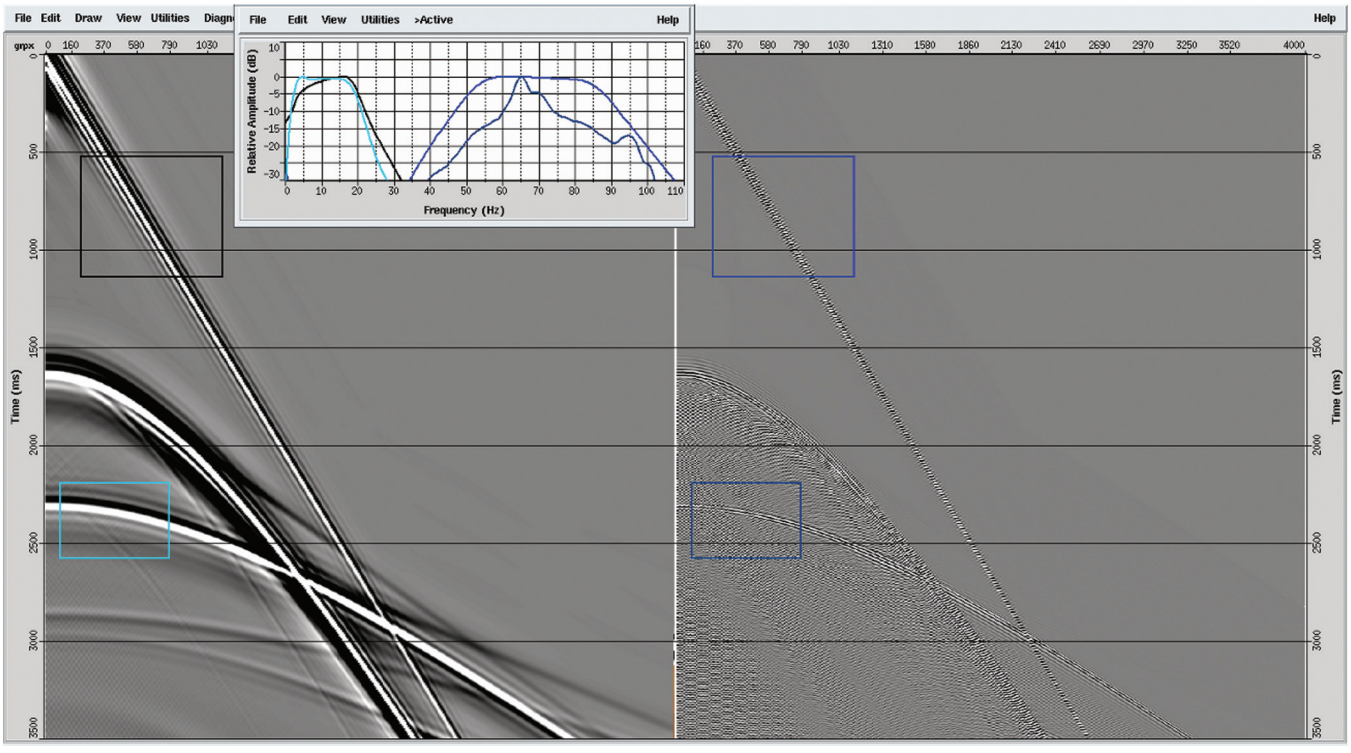


Figure 10. Synthetic reflection data with a 0–10–15–20-Hz trapezium wavelet (left) and a 40–50–80–100-Hz trapezium wavelet (right) from the model of Figure 9. Spectra of the direct wave measured in, respectively, the black and the dark-blue box, and of the 1750- to 3000-m/s interface measured, respectively, in the light-blue and gray box are shown in the top decibel-amplitude-versus-frequency display.

low frequencies. It is interesting to note that the O'Doherty-Anstey theory (Anstey, 1960; O'Doherty and Anstey, 1971) reinforces this, as the wave transmitted through a sequence of nondissipative "sustained cyclic layering" has a "high-frequency cut" and, therefore, the effect of an apparent absorption. When this wave subsequently is reflected at a major sequence boundary, the high-frequency cut effect is doubled on the return path to the receiver, and as a result, low frequencies dominate in the final reflection data. This effect might be present on the left-hand-side of Figure 12, where the rugosity of the basalt diminishes, and the "cyclic layering high-frequency cut" starts to dominate the reflection response.

Absorption is typically assumed to be the dominant reason for imaging problems below gas clouds, but this may not always be the case. The very low velocities due to the gas in the permeable

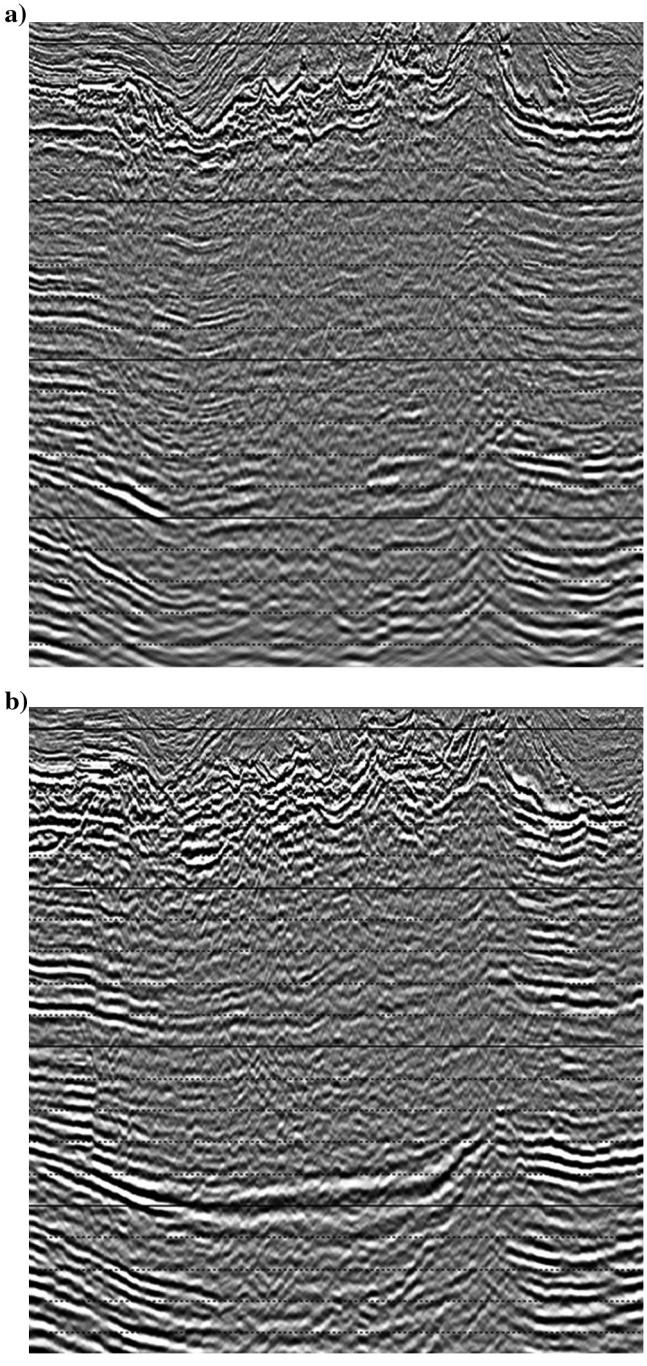


Figure 11. Conventional acquisition (a) and source and receiver broadband acquisition (b).

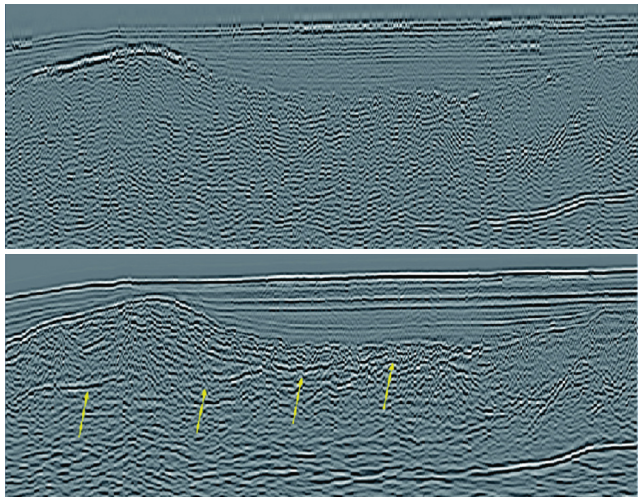


Figure 12. Conventional acquisition (top) and broadband acquisition (bottom) over a basalt pinch-out. Arrows indicate base basalt.

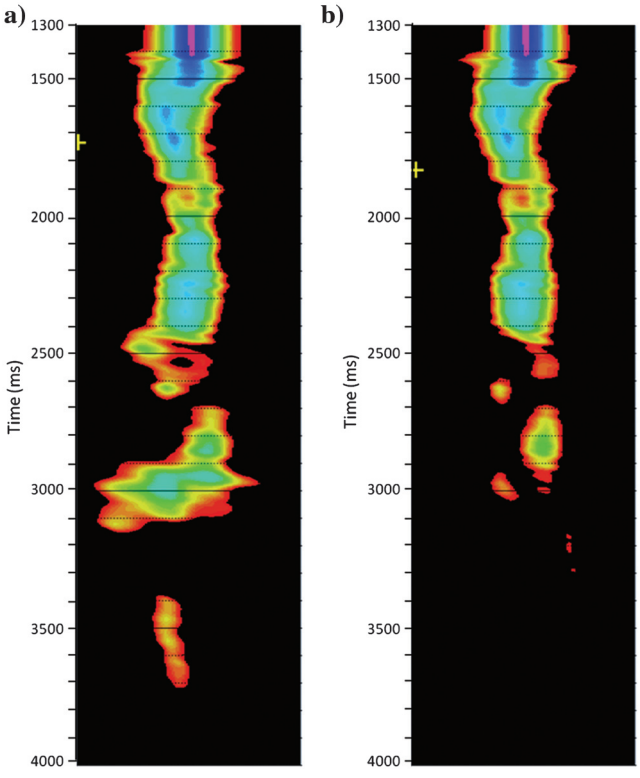


Figure 13. Semblance panel in the middle of the gas cloud: (a) broadband data and (b) the same broadband data low-cut filtered at 9 Hz. The top of the gas cloud is at approximately 1650 ms.

Downloaded 09/15/21 to 69.181.137.94. Redistribution subject to SEG license or copyright; see Terms of Use at http://library.seg.org/page/policies/terms
DOI:10.1190/geo2012-0294.1

Downloaded 09/15/21 to 69.181.137.94. Redistribution subject to SEG license or copyright; see Terms of Use at http://library.seg.org/page/policies/terms
DOI:10.1190/geo2012-0294.1

layers (sometimes less than 1000 m/s) and the much higher velocities in the nonpermeable layers typically create a very complex wavefront. Of course, absorption may play a role, but the real issue may be to derive the velocity model needed to image below the gas cloud. Due to the large velocity contrasts between permeable and nonpermeable layers, the moveout from trace to trace can be so complex that it is impossible to track and pick a coherent event. This is where the very low frequencies come to our aid, because they do permit the picking of coherent events, allowing us to build a velocity model that can subsequently be used to image the full bandwidth data.

We illustrate this with a gas-cloud-dominated example, for which we have acquired standard and broadband data. The difference between the semblance panels with low frequencies and without low frequencies is depicted in Figure 13. The approximate top of the gas cloud is at 1650 ms. Note the difference in the velocity

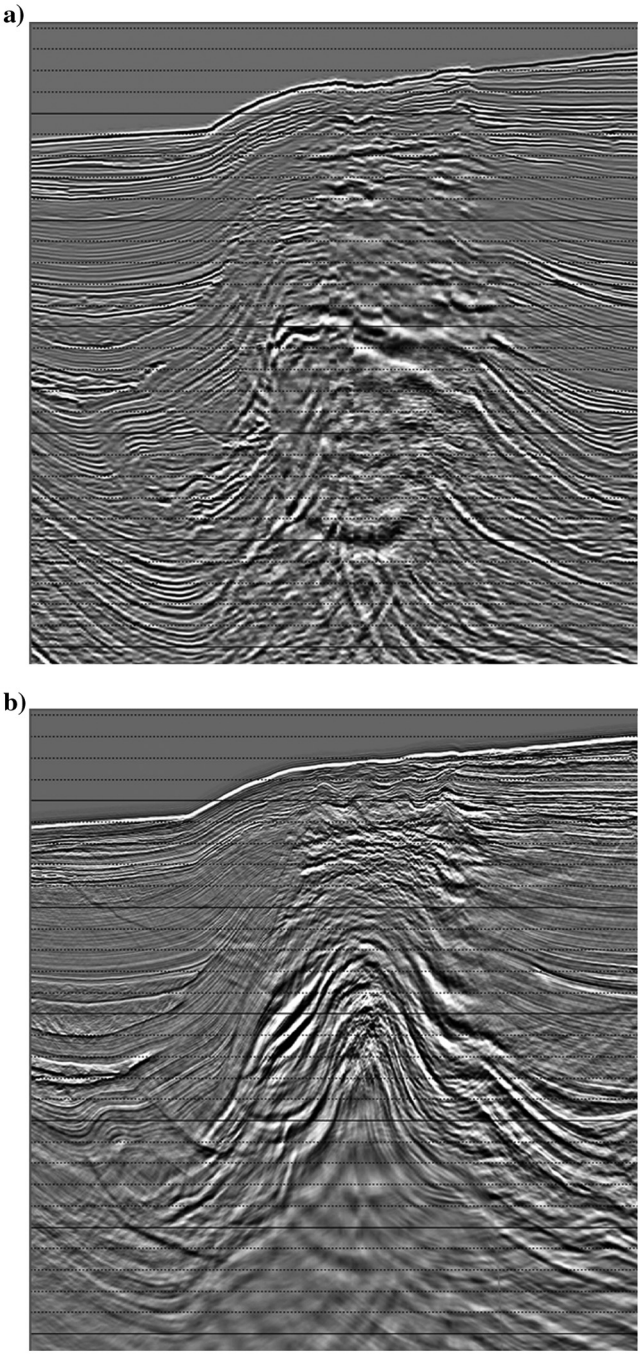


Figure 14. (a) Three-dimensional PSDM based on 3D velocity model building on 3D conventional data and (b) 2D PSDM based on 2D velocity model building of 2D broadband data. Both are displayed in time for comparison.

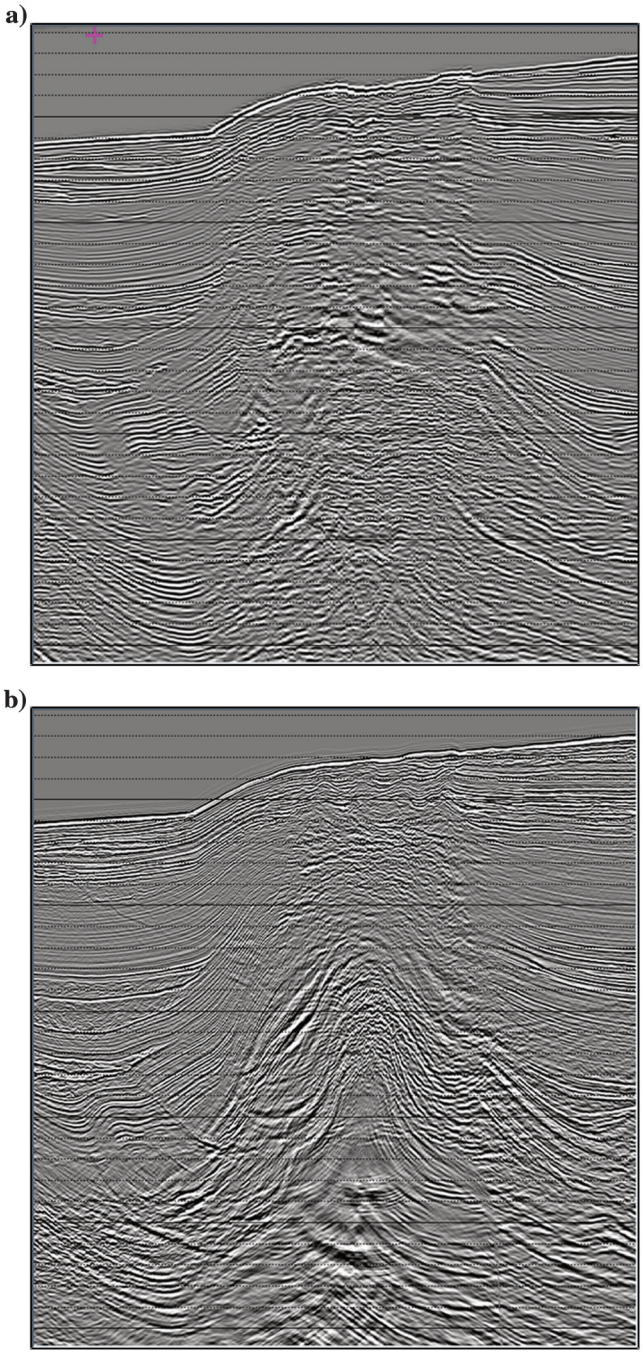


Figure 15. Same as Figure 14 but band-passed to 30–100 Hz: (a) conventional and (b) broadband.

Downloaded 09/15/21 to 69.181.137.94. Redistribution subject to SEG license or copyright; see Terms of Use at http://library.seg.org/page/policies/terms
DOI:10.1190/geo2012-0294.1

trend on the semblance panels below this level. Figure 14 compares a 3D prestack depth migration (PSDM) using the velocity model derived from conventional 3D data and a 2D PSDM using the velocity model derived from 2D broadband data. The large uplift in image quality on the broadband result is due to the different velocity model. This illustrates that absorption and penetration are a lesser issue in this particular case, even though anomalously high absorption values were encountered in this setting and confirmed by well data. Figure 15 shows the same imaging but with data band-passed to 30–100 Hz, indicating that the velocity model derived from the lower frequencies also images the higher frequencies.

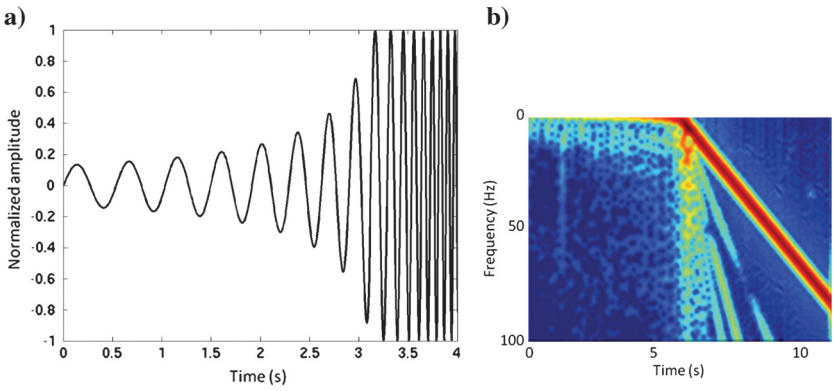


Figure 16. Nonlinear sweep. Left, amplitude as a function of time (first 4 s). Right, frequency as a function of time.

The examples in this section show that seismic imaging benefits from the fact that low frequencies are less affected by scattering, but also that there is a limit to these benefits. We refer to, e.g., Hill et al. (2006) and Moldoveanu et al. (2006) for other examples illustrating the improved penetration at low frequencies. Similarly, we conclude that imaging below a gas cloud may benefit from low frequencies, but our example interestingly shows that this may not only be a penetration or absorption issue. The high frequencies penetrate just as well, but they need the low-frequency-derived imaging velocities to be properly imaged.

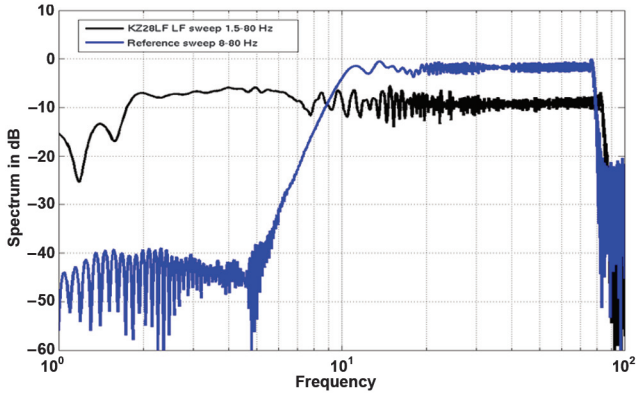


Figure 17. Energy spectrum of standard 8–80-Hz sweep (blue) versus nonlinear sweep (black).

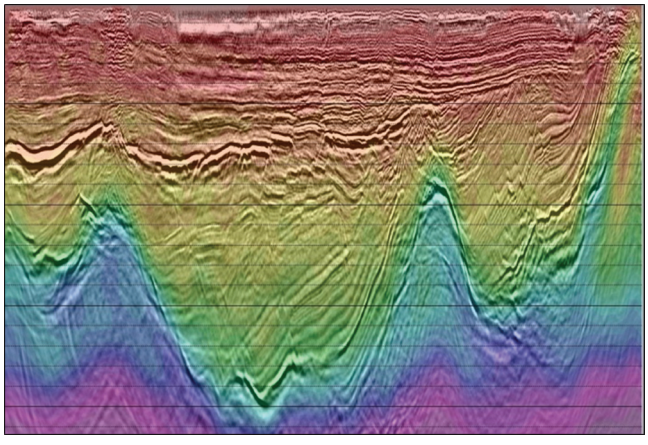


Figure 18. A PSDM image of data on top of velocity model derived by full waveform inversion.

INVERSION FOR VELOCITY AND IMPEDANCE

In this section, we will underline the importance of low frequencies for inversion of earth properties. We will do this by discussing two case studies. The first pertains to velocity estimation by full waveform inversion, and the second pertains to impedance inversion. In both cases, we will conclude that enhancing the bandwidth at the low end can make a large difference.

Our first example is an onshore one with a vibroseis source. Vibroseis trucks normally generate sweeps in a frequency band roughly bounded by 6–7 Hz at the low end and 80 Hz at the high end. Generating lower frequencies is difficult, and there is a simple physical explanation for this based on vibrator mechanics, which dictates that the maximum force exercised by the baseplate of the vibrator scales linearly with the product of reaction mass, piston stroke, and frequency squared:

$$\text{force} \sim (\text{reaction mass}) \times (\text{piston displacement}) \times (\text{frequency squared}). \quad (3)$$

This simple relation tells us that, for a given vibrator, the maximum force scales with the frequency squared and will therefore be low at low frequencies. There are various ways to overcome this, all essentially based on replacing linear sweeps, which spend an equal amount of time at all frequencies, by nonlinear sweeps, which spend more time at the low end of the spectrum; see Bagaini (2008), Baeten et al. (2010), and Wei et al. (2012). We have tested nonlinear sweeps of various lengths (9–12 s), see Figure 16 for a 12-s one. The resulting energy spectrum as measured by a force meter on the baseplate is shown in Figure 17. It has good signal down to ~1.5 Hz. Note that the overall energy level of the nonlinear sweep is somewhat lower than a 6 s, 8–80-Hz reference sweep. This is the price one has to pay for spending more time in the low end of the spectrum.

Downloaded 09/15/21 to 69.181.137.94. Redistribution subject to SEG license or copyright; see Terms of Use at http://library.seg.org/page/policies/terms
DOI:10.1190/geo2012-0294.1

We have acquired a 2D test line with these nonlinear sweep parameters in Inner Mongolia (China) in 2009 (see Plessix et al., 2010). After extensive noise attenuation, we were able to obtain data with good S/N down to 1.5 Hz. We estimated a velocity model with full waveform inversion of all data up to 5 Hz, using a starting model of the form $v = v_0 + kz$. Subsequently, we have imaged the full bandwidth data by running a prestack depth migration with the estimated velocity model. Figure 18 shows that the migration image and velocity model conform well. Other diagnostics (image gathers and comparisons against a sonic well log) also indicate that the full-waveform inversion has been successful.

To demonstrate the impact of the low frequencies, we bandpassed the data and ran full waveform inversion on data with frequencies from 2 to 5 Hz and on data with frequencies from 4.5 to 5 Hz. The resulting velocity models are compared against the earlier one in Figure 19. Clearly, the one obtained from data with the lowest frequency of 2 Hz is already significantly worse than the one obtained from data with the lowest frequency of 1.5 Hz, whereas the one with the lowest frequency of 4.5 Hz bears only a faint resemblance to the 1.5-Hz one. Note that going from 2 to 1.5 Hz as the lowest frequency means adding half an octave of bandwidth, so half a hertz is not as little as it seems. Also, note that we might have obtained better results for the data less rich in low frequencies by using a better starting model. This is underlining the folk knowledge that low frequencies enlarge the basin of attraction for full waveform inversion (Bunks et al., 1995).

Our second example is a marine one. It focuses on the importance of additional low-frequency content in broadband data for impedance inversion. This topic has been discussed by various other authors (e.g., Özdemir, 2009; Reiser and Ribeiro, 2010; Reiser et al., 2011; Soubaras and Lafet, 2011; Michel et al., 2012).

Impedance inversion is usually performed after imaging as the first step toward quantitative interpretation. Typical marine seismic data have frequencies starting at 5–8 Hz, whereas the model obtained from seismic reflection tomography has frequencies up to 2 Hz. The resulting bandgap is usually filled in by using well information: low-passed impedance logs between well locations are interpolated using horizons interpreted on migrated seismic as a guide. If wells are sparse and/or the subsurface is complex, such low-frequency models will, however, be inaccurate. It would obviously be preferable to not have to rely on well-based information and to have good S/N on the frequencies down to ~2 Hz in the data.

We have run impedance inversion on conventional data and on 3D broadband data over two producing reservoirs in the North Sea without adding well information. The results are shown in Figure 20 and clearly show the importance of adding low frequencies. The colors indicate net-to-gross: sands being yellow-red, and shales being blue-green. Field A is located on the right-hand-side of the section and is produced from a thick sand. Field B is located against the flank of a salt dome (left-hand-side of the section) and is produced from an interval with sands from different lithologic units. The sand from field A is also found in field B but much thinner. Because field A has an oil-water contact (OWC) deeper than the structural spillpoint toward field B, it was always assumed that the sands in field A pinch out toward field B, but as Figure 20b shows, this could not be convincingly proven by inversion on the conventional seismic data. The broadband inversion, however, is able to show the pinch-out; it also clearly shows the thick sand in field A, which does not come out as a single thick sand on

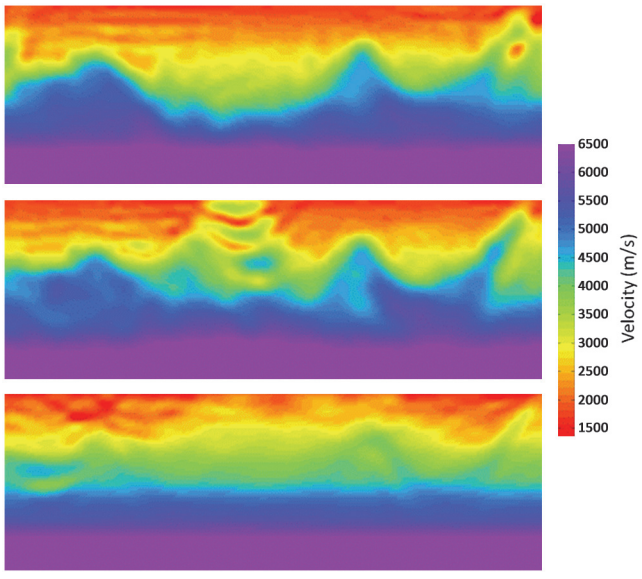


Figure 19. Velocity models obtained from full-waveform inversion in the $v_0 + kz$ starting model and using frequency bands 1.5–5 (top), 2–5 (middle), and 4.5–5 Hz (bottom).

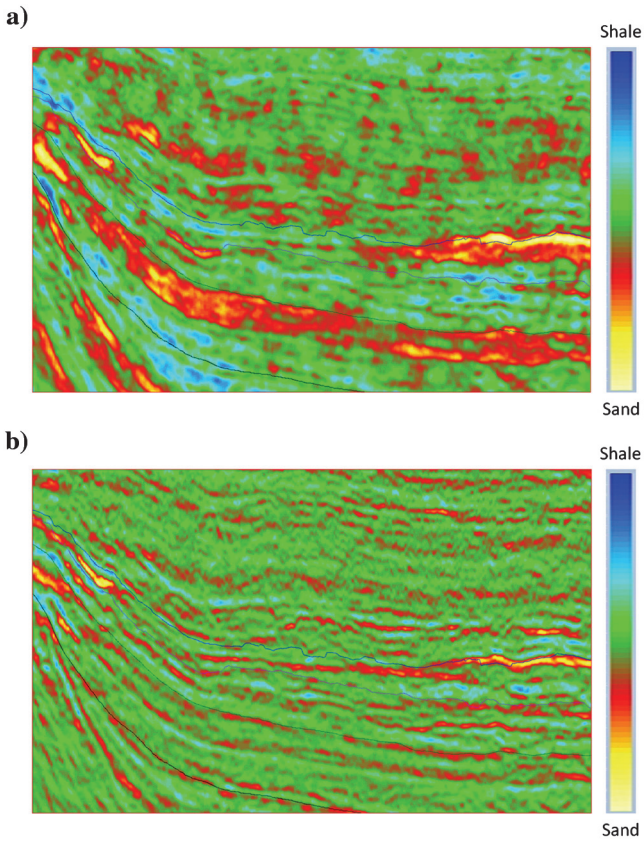


Figure 20. Impedance inversion of (a) broadband data and (b) conventional streamer data. The OWC is deeper than the structural spillpoint. Pinch-out seen on broadband image (top) is a possible explanation. Thick sands are visible on the broadband data.

Downloaded 09/15/21 to 69.181.137.94. Redistribution subject to SEG license or copyright; see Terms of Use at http://library.seg.org/page/policies/terms
DOI:10.1190/geo2012-0294.1

the conventional data. Finally, the lower reservoir found in field B is a thick sandy interval, which is expected to be laterally continuous based on regional geology. The inversion of the broadband data indeed shows this thick sand, whereas that of conventional data do not bring it out.

DISCUSSION

The examples above trigger several questions, such as what could be achieved if we could extend the bandwidth to even lower frequencies and where research and development efforts of the industry should be focusing as far as low frequencies are concerned.

Let us start to answer the second question. There are two obvious elements to this because enhanced low-frequency content depends on the S/N at the low end of the spectrum. The first element addresses the signal aspect by developing dedicated low-frequency sources. The marine airgun has natural limitations at the low end, which are elegantly explained by Hegna and Parkes (2011). This clearly calls for other sources with better signal in the 0–7-Hz band. On land, the industry has already made a significant step in recent years by using nonlinear sweeps with traditional vibrators, thus extending the bandwidth down to ~1.5 Hz. Going down further may require other devices (e.g., Noorlandt et al., 2012). We should realize, of course, that we may not be able to use these everywhere due to the environmental impact of very low frequencies.

The second element is clearly to address the noise part of the S/N. As is well known, background noise grows approximately with frequency to the power −1. Also, at very low frequencies, standard arrays used in land seismic acquisition do not attenuate ground roll anymore, because different geophones essentially sum up signals that are in-phase. A similar effect is caused by very long wavelength ocean waves. In summary, coherent and incoherent noises tend to grow with lower frequencies. Some of these issues can be addressed in acquisition again. For example, towing deeper or using ocean-bottom systems typically leads to much less noise. On land, we may try to improve sampling so that we can construct large digital arrays, capable of attenuating ground roll at low and high frequencies at the same time. A similar approach may be possible with large-scale ocean-bottom acquisition. These improvements in acquisition should go hand in hand with processing technology aiming at improving noise attenuation at low frequencies, e.g., high-fidelity debubbling and/or zero phasing of low-frequency data in preparation for the other processing steps, such as reliable low-frequency surface-related multiple elimination.

There is little doubt that improving the S/N in the 1–7-Hz band by a combination of better acquisition and processing technology is going to be very beneficial, but what could be achieved with even lower frequency content, say below 1 Hz? The answer to this question is, of course, a bit more speculative. In general, at very low frequencies, the earth becomes almost transparent and waves essentially only see the major discontinuities in material parameters plus a velocity profile smoothly increasing with depth. As a consequence, we only observe reflections from the major geologic events (salt, basalt, basement, etc.) in the earth plus diving waves/refractions, the latter to very large offsets. Figures 21 and 22 nicely illustrate this by showing simulated wave propagation and reflection data for normal-, low- and ultralow-frequency source signals in the BP2004 model (Brandsberg-Dahl and Billette, 2005).

From our discussion on resolution, it is hard to see how such extremely low frequencies could contribute to reducing the sidelobes of sedimentary reflections much further, and this is, of course, reinforced by the observation that such low-frequency sedimentary reflections can hardly be observed in a seismogram. The same can be said for impedance inversion on these types of events. What is left is penetration and full-waveform inversion. Exploring the transition between exploration seismic and earthquake seismology, say in the 0.1–1-Hz band, with an eye on these two topics may be interesting. If we could find a cost-effective way to acquire such low-frequency data by a set of very coarsely separated shots and receivers, we might be able to construct a low-frequency model of a basin, which may be interesting for basin modeling and which we could use as a starting model for full-waveform inversion.

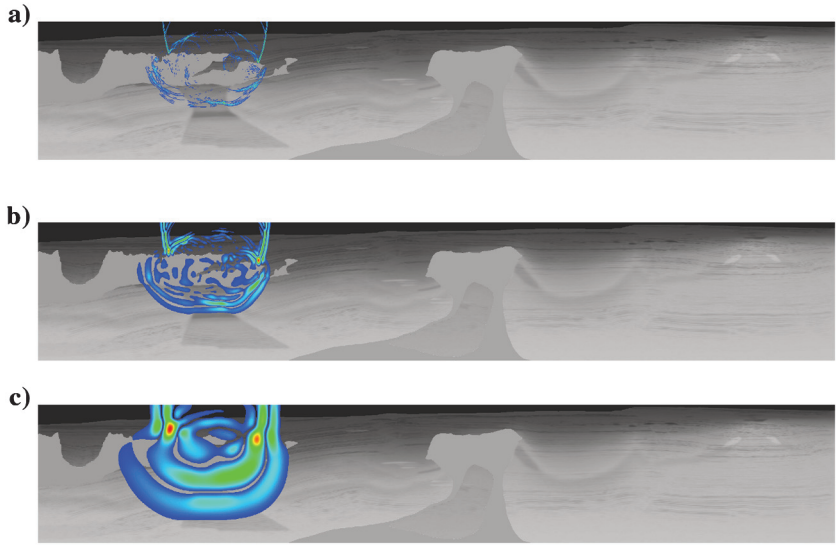


Figure 21. Wave propagation in the BP2004 model at (a) normal, (b) low, and (c) ultralow frequencies.

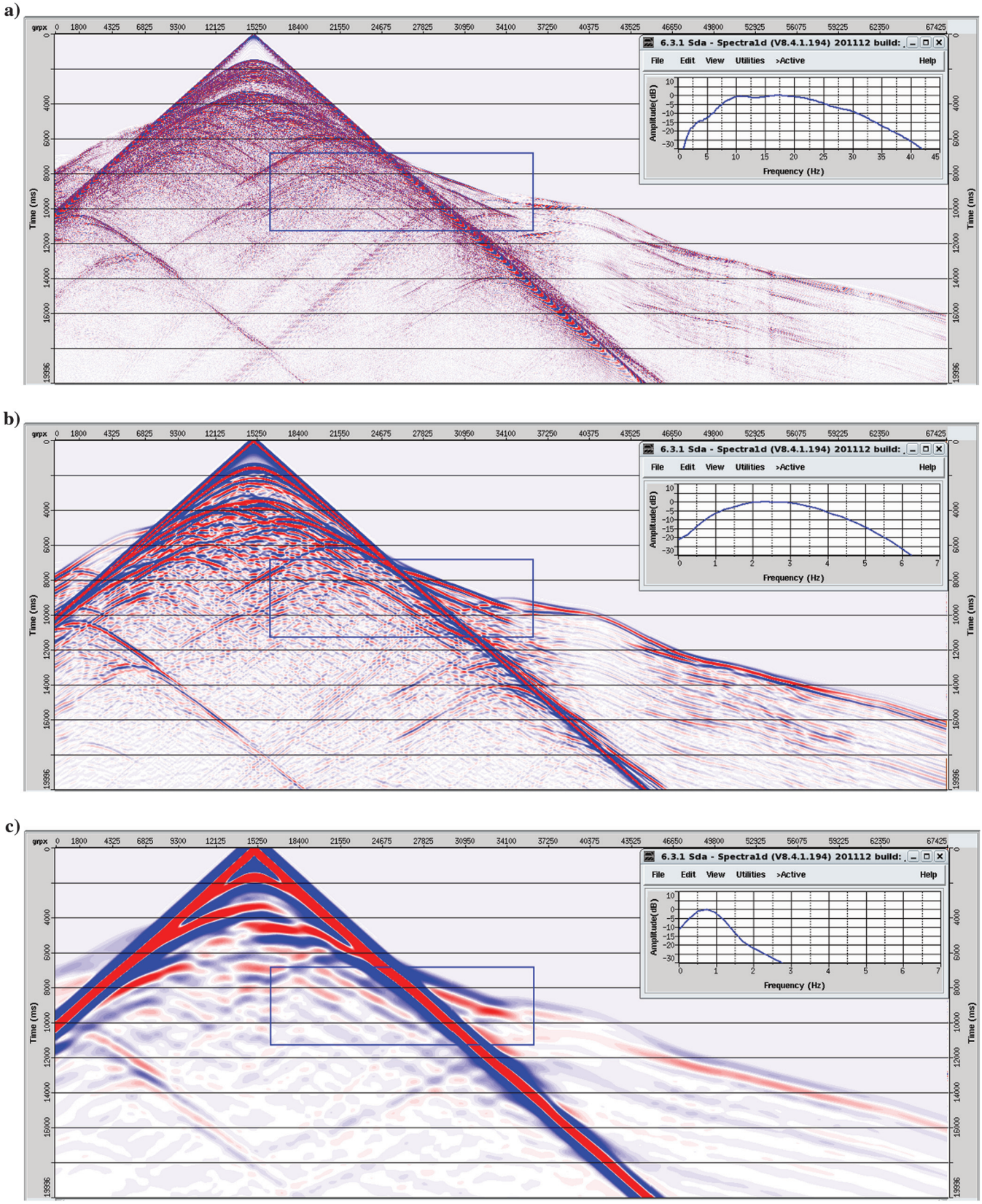


Figure 22. Seismogram of synthetic reflection data in the BP2004 model at (a) normal, (b) low, and (c) ultralow frequencies.

Downloaded 09/15/21 to 69.181.137.94. Redistribution subject to SEG license or copyright; see Terms of Use at http://library.seg.org/page/policies/terms
DOI:10.1190/geo2012-0294.1

Downloaded 09/15/21 to 69.181.137.94. Redistribution subject to SEG license or copyright; see Terms of Use at http://library.seg.org/page/policies/terms
DOI:10.1190/geo2012-0294.1

CONCLUSIONS

We have reviewed the well-known arguments explaining why low frequencies contribute to better resolution, penetration, and inversion: (1) extending the bandwidth of the recorded seismic signal at the low end of the spectrum leads to less sidelobes on the wavelet, (2) low frequencies scatter less and suffer less from absorption in the earth, so they penetrate deeper, (3) at low frequencies, the number of local minima in least-squares misfit functions used in full waveform inversion is smaller, so we have a better chance to converge to the true earth model with this method, and (4) a richer low-frequency content may eliminate the need for well-derived velocities to fill the traditional bandgap in impedance inversion.

We have underpinned these arguments by means of case studies with recently acquired broadband data, which are especially rich in low frequencies and compared the results against those obtained with data that have poorer low-frequency content. These case studies clearly illustrate these arguments and show that the industry has made significant strides forward in terms of extending the bandwidth at the lower end of the spectrum over the past five years or so, while maintaining and extending the bandwidth at the high end at the same time. We feel there is no reason to believe that the limits of extracting value out of the low end of the seismic spectrum are in sight yet. To explore the benefits further, far more research and development are needed, especially in the area of low-frequency sources generating known and stable phases and in processing technology aiming at S/N enhancement for the low frequencies.

ACKNOWLEDGMENTS

We would like to thank WesternGeco, PGS, CGGVeritas, and BGP, suppliers of this technology, for their permission to use some of their data. Within our own company, we would like to thank H. Dankbaar for providing help with the impedance inversion example in Figure 20 and C. Corcoran and J. Sheiman for their support to deploy this technology globally.

REFERENCES

Aki, K., and P. Richards, 1980, Quantitative seismology, vol. II: W.H. Freeman.

Anstey, N. A., 1960, Attacking the problems of the synthetic seismogram: Geophysical Prospecting, **8**, 242–259, doi: 10.1111/j.1365-2478.1960.tb01500.x.

Baeten, G., A. Egreteau, J. Gibson, F. Lin, P. Maxwell, and J. J. Sallas, 2010, Low-frequency generation using seismic vibrators: 72nd Annual International Conference and Exhibition, EAGE, Extended Abstracts, B015.

Bagaini, C., 2008, Low-frequency vibroseis data with maximum displacement sweeps: The Leading Edge, **27**, 582–591, doi: 10.1190/1.2919575.

Brandsberg-Dahl, S., and F. J. Billette, 2005, The 2004 BP velocity benchmark: 67th Annual International Conference and Exhibition, EAGE, Extended Abstracts, B035.

Bremmer, H., 1951, The W. K. B. approximation as a first order term of a geometric-optical series: Communications in Pure and Applied Mathematics, **4**, 105–115.

Bunks, C., F. M. Saleck, S. Zaleski, and G. Chavent, 1995, Multiscale seismic waveform inversion: Geophysics, **60**, 1457–1473, doi: 10.1190/1.1443880.

Caprioli, P. B. A., A. K. Özdemir, A. Özbek, E. Kragh, D. J. van Manen, P. A. F. Christie, and J. O. A. Robertsson, 2012, Combination of multi-component streamer pressure and vertical particle velocity —Theory and application to data: 74th Annual International Conference and Exhibition, EAGE, Extended Abstracts, A033.

Carlson, D., A. Long, W. Söllner, H. Tabti, R. Tenghamn, and N. Lunde, 2007a, Increased resolution and penetration from a towed dual-sensor streamer: First Break, **25**, 71–77.

Carlson, D., W. Söllner, H. Tabti, E. Brox, and M. Widmaier, 2007b, Increased resolution of seismic data from a dual-sensor streamer cable: 77th Annual International Meeting, SEG, Expanded Abstracts, 994–998.

Hegna, S., and G. Parkes, 2011, The low frequency output of marine air-gun arrays: 81st Annual International Meeting, SEG, Expanded Abstracts, 77–81.

Hill, D., L. Combee, and J. Bacon, 2006, Over/under acquisition and data processing: The next quantum leap in seismic technology?: First Break, **24**, 81–96.

Kallweit, R. S., and L. C. Wood, 1982, The limits of resolution of zero-phase wavelets: Geophysics, **47**, 1035–1046, doi: 10.1190/1.1441367.

Lippmann, B. A., and J. Schwinger, 1950, Variational principles for scattering processes: Physical Review, **79**, 469–480, doi: 10.1103/PhysRev.79.469.

Michel, L., Y. Lafet, R. Sablon, D. Russier, and R. Hanumantha, 2012, Variable depth streamer — Benefits for rock property inversion: 74th Annual International Conference and Exhibition, EAGE, Extended Abstracts.

Moldoveanu, N., L. Combee, M. Egan, W. Abriel, and G. Hampson, 2006, Over/under towed-streamer acquisition: A method to extend the seismic bandwidth to both higher and lower frequencies: 76th Annual International Meeting, SEG, Expanded Abstracts, 10–15.

Morse, P. M., and H. Feshbach, 1953, Methods of theoretical physics: McGraw-Hill Book Company.

Noorlandt, R. P., G. G. Drijkoningen, and R. M. Schneider, 2012, A seismic vertical vibrator driven by linear motors: 74th Annual International Conference and Exhibition, EAGE, Extended Abstracts, P061.

O'Doherty, R. F., and N. A. Anstey, 1971, Reflections on amplitudes: Geophysical Prospecting, **19**, 430–458, doi: 10.1111/j.1365-2478.1971.tb00610.x.

Özdemir, H., 2009, Unbiased deterministic seismic inversion: More seismic, less model: First Break, **27**, 43–50.

Parkes, G., and S. Hegna, 2011, A marine seismic acquisition system that provides a full "ghost-free" solution: 81st Annual International Meeting, SEG, Expanded Abstracts, 37–41.

Plessix, R.-E., G. Baeten, J. W. de Maag, M. Klaassen, Z. Rujie, and T. Zhifei, 2010, Application of acoustic full waveform inversion to a low-frequency large-offset land data set: 80th Annual International Meeting, SEG, Expanded Abstracts, 930–934.

Reiser, C., E. Anderson, Y. Balabekov, and F. Engelmark, 2011, Broadband seismic: The ultimate input for quantitative interpretation?: 81st Annual International Meeting, SEG, Expanded Abstracts, 1825–1829.

Reiser, C., and C. Ribeiro, 2010, Impact of the dual-sensor acquisition on reservoir characterization studies: 80th Annual International Meeting, SEG, Expanded Abstracts, 2371–2375.

Soubaras, R., 2010, Deghosting by joint deconvolution of a migration and a mirror migration: 80th Annual International Meeting, SEG, Expanded Abstracts, 3406–3410.

Soubaras, R., and R. Dowle, 2010, Variable-depth streamer — A broadband marine solution: First Break, **28**, 89–96.

Soubaras, R., and Y. Lafet, 2011, Variable-depth streamer acquisition: Broadband data for imaging and inversion: 81st Annual International Meeting, SEG, Expanded Abstracts, 2364–2368.

Tenghamn, R., S. Vaage, and C. Borresen, 2007, A dual-sensor towed marine streamer: Its viable implementation and initial results: 77th Annual International Meeting, SEG, Expanded Abstracts, 989–993.

Velzeboer, C. J., 1981, The theoretical response of sedimentary sequences: Geophysics, **46**, 843–853, doi: 10.1190/1.1441222.

Wei, Z., M. A. Hall, and T. F. Phillips, 2012, Geophysical benefits from an improved seismic vibrator: Geophysical Prospecting, **60**, 466–479, doi: 10.1111/j.1365-2478.2011.01008.x.

Widess, M. B., 1973, How thin is a thin bed?: Geophysics, **38**, 1176–1180, doi: 10.1190/1.1440403.

Wu, R. S., 2003, Wave propagation, scattering and imaging using dual-domain one-way and one-return propagators: Pure and Applied Geophysics, **160**, 509–539, doi: 10.1007/PL00012548.